JOURNAL OF PROPULSION AND POWER
Vol. 23, No. 1, January–February 2007

Whole Ion Optics Gridlet Simulations Using a Hybrid-Grid Immersed-Finite-Element Particle-in-Cell Code

R. Kafafy* and J. Wang†
Virginia Polytechnic Institute and State University, Blacksburg, Virginia 24061-0203

DOI: 10.2514/1.21346

A new model is developed for three-dimensional global simulations of plasma flow in an entire subscale ion optics. This model explicitly includes apertures located near the edge of the grid surface and fully accounts for the effects of multiple ion beamlets and geometric asymmetry. This model is based on a new algorithm, the streamline hybrid-grid immersed-finite-element particle-in-cell. This algorithm is capable of achieving the same accuracy as an unstructured body-fit mesh-based particle-in-cell with a faster computational speed. Simulation results are presented to understand the plasma sheath upstream of the screen grid, direct impingement of beam ions, the crossover limit, the perveance limit, and the electron backstreaming onset.

Nomenclature

e	=	electron charge
$\boldsymbol{F}$	=	force vector
$\boldsymbol{I}$	=	current
k	=	Boltzmann constant
m	=	mass
q	=	charge
T	=	temperature
t	=	time
$\boldsymbol{v}$	=	velocity vector
$\boldsymbol{x}$	=	position vector
β	=	IFE mesh stretching parameter
ϵ_0	=	electric permittivity of vacuum
λ_D	=	Debye length
ρ	=	charge density
Φ	=	electrostatic potential

Subscripts

a	=	accelerator grid
b	=	beamlet
cc	=	center-to-center
e	=	electron
g	=	gap between ion optics grids
i	=	ion, or impingement
s	=	screen grid
w	=	grid wall
0	=	upstream plasma condition
∞	=	downstream plasma condition

I. Introduction

THERE have been significant efforts in developing ion optics models for ion thruster research and development in recent years. The nature of plasma flow in ion optics renders particle-in-cell (PIC) [1] based models, which simulate a collisionless plasma by solving plasma particle trajectories, space charge, and the electric field self-consistently as the most appropriate approach for ion optics modeling. Numerous PIC-based ion optics simulation codes have been developed (see, for example, [2–17] and references therein). Whereas earlier studies have focused on the physics of a single beamlet, recent studies have also begun to use ion optics models to predict the behavior of entire ion optics.

A particularly important issue in ion optics design is to understand the behavior of the accelerator grid current. The accel grid current defines the operational envelope of an ion optics. Under normal operating conditions, the ions in the discharge plasma upstream of the screen grid should form focused ion beamlets when extracted and accelerated through the optics. However, if the discharge plasma density is too low, the ion beamlet may become overfocused by the upstream sheath, resulting in crossover ion impingement on the acceleration grid. On the other hand, if the discharge plasma density is too high, the ion beamlet may become underfocused, resulting in direct interception of beam ions by the acceleration grid (perveance limit). As thruster operation that results in direct impingement will cause excessive sputtering erosion of the acceleration grid, accurate predictions of these limits are needed to ensure long-term, trouble-free operation.

Most existing ion optics models are either axisymmetric models or three-dimensional models constructed for a cross section of one twelfth of a single aperture (a 30 by 60 deg right-triangle cross section) using the six-fold hexagonal symmetry of the aperture array. Because of the inherent symmetric boundary conditions, existing models are suitable for local simulations of a single ion beamlet for an aperture located near the center of the optics grid. Existing modeling predictions of important ion optics parameters, such as the crossover limit, perveance limit, and backstreaming limit, are all based on extrapolations of single beamlet simulations, where one uses different upstream plasma conditions to represent apertures at different locations on the grid surface. Wang et al. [10] presented a fully three-dimensional model which allows multiple apertures to be included in the simulation domain. However, simulations were performed only for two quarter-apertures in the center of the optics grid due to computational constrains. Currently, no existing models are capable of global simulations of an entire ion optics. No simulation studies have been performed to directly predict accel grid current behavior for an entire optics.

This paper presents the first three-dimensional model designed for global simulations of an entire subscale ion optics. This model explicitly includes apertures located near the edge of optics grid and the insulator spacer in between the grids in the simulation domain, and fully accounts for the effects that are not included in a single beamlet model, such as geometric asymmetry and multiple ion beamlets.

Received 23 November 2005; revision received 5 May 2006; accepted for publication 7 May 2006.

*Postdoctoral Research Associate, Department of Aerospace and Ocean Engineering; rkafafy@vt.edu. Member AIAA.

†Associate Professor, Department of Aerospace and Ocean Engineering; jowang@vt.edu. Associate Fellow AIAA.

Subscale ion optics gridlets were often used to investigate the behavior of full-sized optics in experimental studies. For instance, various experiments were carried out recently using subscale gridlets with 1, 7, 19, and 37 apertures to help the development of the NEXT ion optics [18,19]. In this paper, the new ion optics model is applied to perform global simulations of plasma flow in an entire subscale ion optics gridlet and to predict the crossover and the perveance limits.

Ion optics simulation results sensitively depend upon the upstream and downstream plasma conditions. It is essential in a simulation to use a sufficiently large simulation domain so that both the upstream and downstream boundary conditions can be resolved properly [10]. Moreover, it is also obvious that the boundary effects from the ion optics grid wall on the electric field must be resolved accurately in a simulation. The accuracy required by the electric field solution and the computational speed required for large-size simulations present a major challenge in the design of PIC code for whole ion optics modeling. All current ion optics models use either standard finite difference or finite element methods to solve the electric field. In the presence of a complex boundary, many existing numerical methods based on either the finite element or the finite difference approach using unstructured mesh can be applied to solve the electric field accurately. However, an ion optics model using these field solve methods can be computationally expensive. A PIC code is computationally most efficient when using a Cartesian mesh, but a standard finite difference Cartesian mesh-based field solver will lose accuracy in the vicinity of an irregular boundary.

Recently, a new field solution algorithm, the immersed-finite-element (IFE), is developed by Kafafy et al. [20] for use in large-scale PIC simulations of problems involving complex boundary conditions. The IFE algorithm allows one to use a structured Cartesian mesh for problems involving complex geometric boundaries. The IFE algorithm is incorporated into PIC to develop the IFE-PIC algorithm [21], which uses the immersed-finite-element formulation to solve the electric field on a Cartesian-tetrahedral mesh and the standard PIC to push particles. It is shown that this algorithm is capable of solving the electric field with the same accuracy as an unstructured mesh-based method [20] and that the computational speed of IFE-PIC is similar to that of a standard, finite-difference-based PIC [22]. In [23], Kafafy and Wang further developed a new meshing technique, the hybrid-grid, to decouple the mesh of the IFE field solver and the mesh of PIC. The primary mesh used by the IFE field solver is allowed to stretch according to the local potential gradient and plasma condition. The application of the hybrid-grid reduces the number of elements used by the IFE field solver in the far-field region and thus further reduces both the computation time and the memory requirement for simulations of nonuniform plasma. The ion optics model presented in this paper is based on the hybrid-grid immersed-finite-element particle-in-cell (HG-IFE-PIC) algorithm. A streamline simplification of the beam ions is also incorporated to further reduce the computational time and memory requirement. We find that the resulting ion optics code is highly efficient and allows whole ion optics simulations performed on regular PCs.

Section II describes the streamline HG-IFE-PIC algorithm. Section III presents numerical tests of the algorithm. Section IV discusses the simulation model. Section V discusses simulation results. Section VI contains a summary and conclusions.

II. Algorithm

A. IFE-PIC

The ion optics model presented in this paper is developed based on a 3-D PIC code for ion optics by Wang et al. [10,24] and the recently developed 3-D IFE method [20]. The dynamics of the macroparticles, distribution of the space charge, and electrostatic fields are all solved simultaneously and self-consistently. In the IFE-PIC code, the Poisson's equation is solved for the electrostatic field using a 3-D IFE field solver. The IFE field solver is based on the immersed-finite-element method [20,25,26]. Unlike body-fitted, unstructured mesh-based field solvers, the IFE solver treats the ion optics as part of the simulation domain and solves the electric field using the "interface" concept. The major attraction of this method is that it allows the use of a Cartesian-based tetrahedral mesh, which greatly simplifies the search for macroparticle locations and particle-mesh interpolations for PIC, while retaining the numerical accuracy associated with body-fitted field solvers when complex boundaries are encountered.

The idea of using a Cartesian mesh and the finite element approach to model complex geometries was also used by Mandell et al. [27,28] where the details of small objects are captured by surrounding them with a fine primary body-fit grid nested in an outer coarser grid. The standard finite element method is used to solve the Poisson's equation. We note, however, the IFE method is completely different from the method discussed in [27,28]. In IFE, the solution mesh used is independent of the object shape and location. The elements used by IFE include 1) interface elements whose interiors are cut through by the object and 2) noninterface elements. In a noninterface element, the standard linear local nodal basis functions are used to span the local finite element space. In an interface element, the electric field jump condition across object boundary is used to develop the IFE basis functions. The details of the IFE method are discussed in [20,29].

Any structured mesh may be used to solve a problem with a complicated interface. If the simulation domain is of a rectangular shape, one naturally chooses a 3-D Cartesian mesh with brick or tetrahedral elements. Concerning the intersection topology of interface cells, we find that a tetrahedral element possesses favorable topological features compared with a brick element while keeping the total number of mesh nodes the same. Hence, the IFE-PIC code in this paper uses a Cartesian-tetrahedral mesh. Each Cartesian cell is divided into five tetrahedral elements as shown in Fig. 1.

Following the same procedure in standard finite element method, the solution space in the IFE method is discretized using a finite number of local basis functions defined on each cell of the mesh. By investigating the possible intersection topologies of a typical tetrahedral element, we find that it is necessary to consider only two possible intersection topologies, assuming that the mesh size is sufficiently small compared to the interface surface curvature (see Fig. 2).

1) Three-edge cut: The interface surface Γ intersects with the edges of the tetrahedron T at three distinct points (P_1, P_2, and P_3) which are not on the same face of T.

2) Four-edge cut: The interface surface Γ intersects with the edges of the tetrahedron at four distinct points (P_1, P_2, P_3, and P_4) on four different edges, and each three of these intersection points are not on a line.

B. HG-IFE-PIC

In the hybrid-grid IFE-PIC (HG-IFE-PIC), we allow the IFE and the PIC mesh nodes to be displaced from each other instead of being collocated. We keep the uniform Cartesian mesh for PIC but stretch the primary IFE mesh according to the local potential and plasma gradients. This allows us to use fewer elements and mesh nodes to

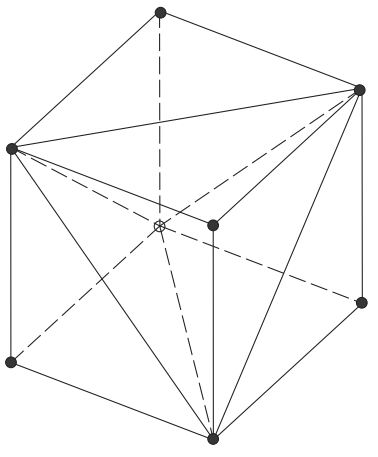

Fig. 1 Partitioning of a Cartesian cell into five tetrahedra.

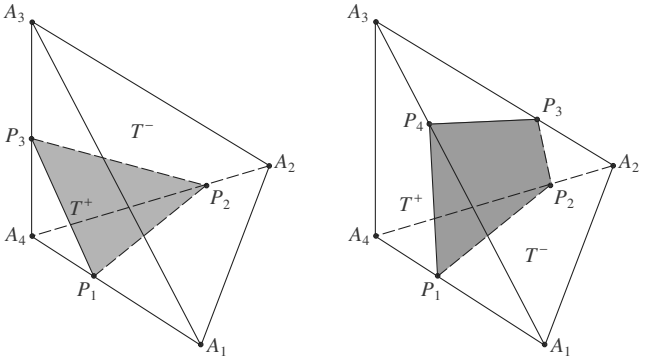

a) Three-edge cut **b) Four-edge cut**

Fig. 2 Intersection topology.

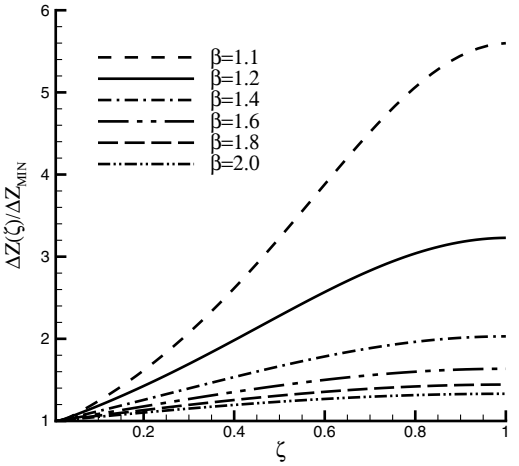

Fig. 3 Stretched cell length for various mesh stretching parameter β. (Number of mesh points used for this plot is $N + 1 = 76$.)

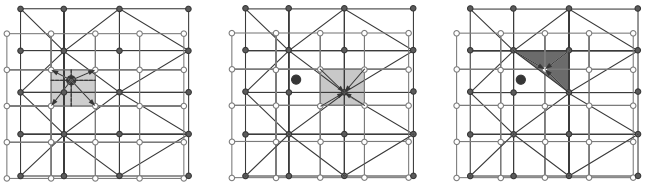

a) Particle-PIC deposition **b) PIC-IFE interpolation** **c) IFE-PIC interpolation**

Fig. 4 Interpolation procedure for a hybrid-grid IFE-PIC. The PIC mesh is shown in light gray and the IFE mesh in dark gray.

solve the same field problem with IFE. The details of HG-IFE-PIC are discussed in [23]

When applied to simulate a nonuniform plasma problem, the IFE mesh stretching follows the local potential and plasma density gradients. The mesh can be stretched in each coordinate independently. In the ion optics model, the IFE mesh is stretched only in the beam ion flow direction (the z) according to the following stretching rule [30]

$$\frac{z(\xi) - z_0}{L} = \frac{\beta + 1 - (\beta - 1)[(\beta + 1)/(\beta - 1)]^{1-\xi}}{[(\beta + 1)/(\beta - 1)]^{1-\xi} + 1} \tag{1}$$

where z is the physical coordinate with $z_0 \le z \le z_0 + L$, ξ is the logical coordinate with $0 \le \xi \le 1$, and β is a stretching parameter with $\beta > 1$. $\beta \to \infty$ means no stretching and $\beta \to 1$ means infinite stretching. If the domain from z_0 to $z_0 + L$ is discretized using $N + 1$ mesh points, then the logical coordinates of these mesh points are

$$\xi(i) = \frac{i - 1}{N}, \qquad i = 1 \text{ to } N + 1 \tag{2}$$

and their physical coordinates are given by Eq. (1). Note that

$$z_{i=1} = z(\xi = 0) = z_0, \qquad z_{i=N+1} = z(\xi = 1) = z_0 + L \tag{3}$$

The cell length in the physical domain, $\Delta z(\xi) = z_{i+1} - z_i$, is a function of ξ, β, and the number of mesh points N. Figure 3 plots the cell length $\Delta z(\xi)$ normalized by the minimum cell length, $\Delta z_{\min} = z_2 - z_1$, for various β.

The HG-IFE-PIC code tracks the particles in the PIC mesh and maintains the standard charge deposit and field interpolation between particles and the PIC mesh nodes. Two additional mesh-to-mesh interpolations are used to pass the information between PIC mesh and the IFE mesh. Particle charges deposited to PIC mesh nodes are interpolated to the IFE mesh using the IFE local basis functions. This requires us to have an IFE-PIC mesh connectivity array which determines the IFE mesh element in which each PIC mesh node occurs. After solving the field equation on the IFE mesh, the field quantities are interpolated back to the particle locations through the IFE local basis functions using a reversed interpolation procedure (see Fig. 4).

C. Streamline PIC

In a regular PIC simulation, one follows all the macroparticles used to represent the plasma and solves the electric field after each particle push step. A typical 3-D ion optics simulation using the regular PIC method would typically require the use of more than 10 million particles to represent the beamlet ions and a very long computation time as the transient state is also being resolved.

The physics of the ion beamlet is dominated by the acceleration of very cold beam ions in an applied electrostatic field. The random motion of the beam ions and the transient effects are not important. To a good approximation, the beamlet profile may be resolved only using the steady-state streamlines generated by the beam ions in a simulation. Hence, the regular PIC method is further modified. In the ion beamlet simulation, rather than following all the macroparticles, we only track the streamlines generated by macroparticles injected at the upstream boundary. A similar approach is used in Arakawa and Nakano [4], Nakayama and Wilbur [31] and Brophy et al. [32] which also neglect the random motion of beamlet ions and consider only the steady-state beam ion trajectories.

The simulation loop begins with the injection of one slice of simulation particles at the upstream boundary and ends when all the particles leave the simulation domain. The particles are uniformly distributed in the injection slice. As the particles are pushed through the simulation domain, they deposit their charges to the mesh points. Then the electric field is solved once all streamlines are updated. The simulation loop is repeated until the beamlet profile is converged. The flowchart of the streamline PIC algorithm is shown in Fig. 5.

The beamlet profile is considered converged when the change in the potential and ion density between two successive loops becomes smaller than a predetermined criterion. The change in potential and ion density may be considered as the error in the solution. The root mean square (rms) and the maximum (max) of the difference in each quantity are calculated from

$$\text{rms}\,(\Delta \boldsymbol{X}^n) = \sqrt{\frac{1}{N}\sum_{i=1}^{N}\left(\boldsymbol{X}_i^{n+1} - \boldsymbol{X}_i^n\right)^2} \tag{4}$$

$$\max(\Delta \boldsymbol{X}^n) = \max_{i=1}^{N} |\boldsymbol{X}_i^{n+1} - \boldsymbol{X}_i^n| \tag{5}$$

where n is the iteration number, i is mesh node index, and N is the total number of mesh nodes. Then, the stopping criteria may be given as

$$\text{rms}\,(\Delta \Phi^n) \le \epsilon\, \text{rms}(\Delta \Phi^0) \tag{6}$$

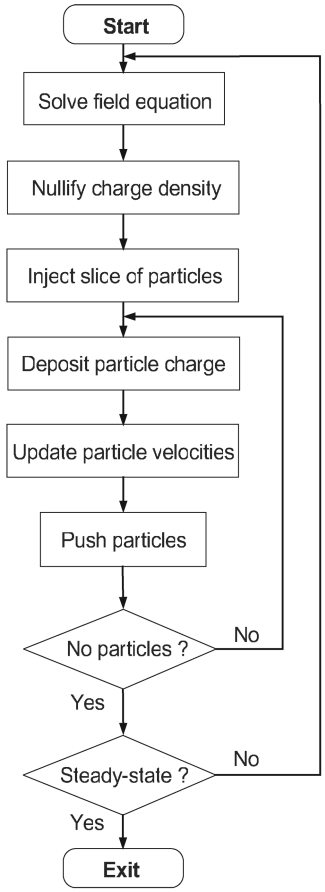

Fig. 5 A flowchart of the streamline PIC algorithm.

$$\text{rms}\,(\Delta\rho^n) \le \epsilon\,\text{rms}(\Delta\rho^0) \tag{7}$$

$$\max(\Delta\Phi^n) \le \epsilon\,\max(\Delta\Phi^0) \tag{8}$$

$$\max(\Delta\rho^n) \le \epsilon\,\max(\Delta\rho^0) \tag{9}$$

where ϵ is an error tolerance. A satisfactory convergence is achieved when the overall beamlet properties, such as beamlet current, impingement current limits, and electron backstreaming onset, are reasonably fixed. Based on numerical tests, we found that $\epsilon = 10^{-3}$ represents a satisfactory convergence criteria. A typical convergence history of a steady-state PIC ion optics simulation is shown in Fig. 6, from which we notice that convergence is obtained in about 20 simulation loops.

III. Numerical Tests of Streamline HG-IFE-PIC

A series of numerical experiments was carried out to assess the accuracy of the new streamline HG-IFE-PIC model. This section presents results from two numerical tests. The first test is to validate the streamline PIC against a standard PIC. The second test is to investigate the effect of the stretching parameter of the hybrid grid.

For both numerical tests, we consider a simulation of an ion beamlet through a single aperture of the ion optics gridlet to be studied in the next section. The simulation setup, which is discussed in details in [10], is a simulation domain including two quarter-apertures (Fig. 7). Beam ion particles are injected from the upstream boundary surface. The upstream boundary is immersed in the discharge plasma and hence has a fixed potential equal to the plasma potential. All other boundaries have Neumann boundary conditions. The IFE mesh used by the new HG-IFE-PIC model is shown in Fig. 8. The ion optics parameters are given in the next section. The simulation parameters such as mesh resolution and domain size are also discussed in the next section.

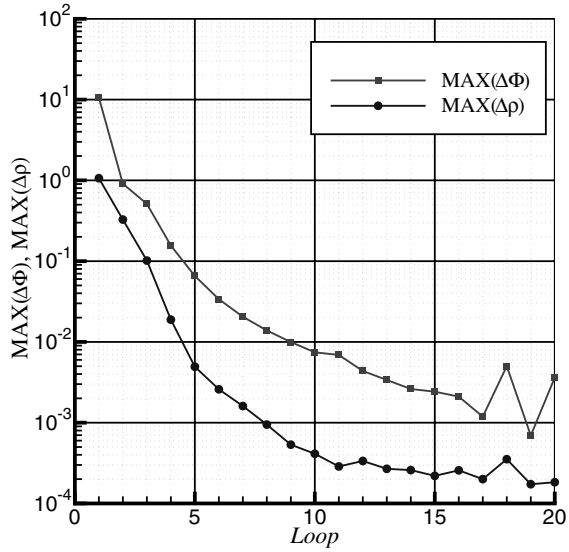

a) *MAX* error

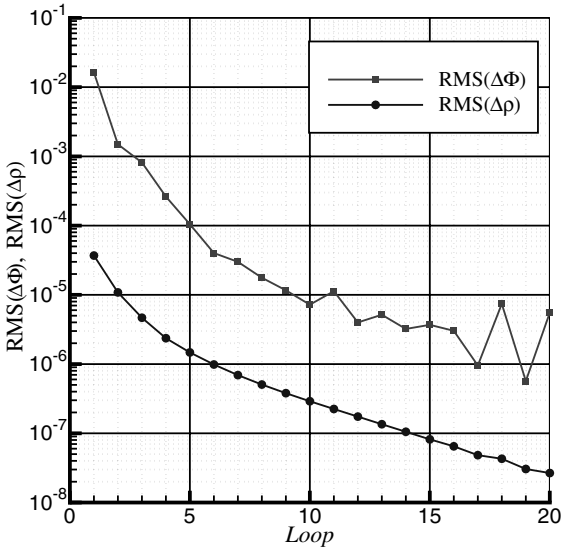

b) *RMS* error

Fig. 6 Convergence history of the streamline HG-IFE-PIC simulation at $n_0 = 0.05 \times 10^{17}$ m^{-3}.

A. Streamline PIC vs Standard PIC

We first run the simulation using both the streamline PIC algorithm and the standard PIC algorithm to investigate the effects of neglecting the random motion of the beam ions in the streamline approximation. Figures 9 and 10 compare the potential and ion density profiles of a single beamlet obtained by the standard PIC simulation against that obtained by the streamline PIC simulation. (The simulation data are mirrored about the y–z plane to illustrate the whole beamlet profile through a single aperture.) These simulations are performed at three selected upstream plasma densities: $n_0 = 0.05 \times 10^{17}$, 1.0×10^{17}, and 14.0×10^{17} m^{-3}. As will be discussed in the next section, these densities represent crossover, nominal, and perveance conditions for the ion optics model considered, respectively. The potential contour lines are shown for values from -210 to 1790 V with a step of 200 V. The potential contour lines at $\Phi = -140, 0, 1780$, and 1795 V are also shown. The beamlet ion density contours in the plots are normalized by the nominal discharge plasma density.

Comparing the plots in Figs. 9 and 10, we find that the potential lines from both models are almost the same. The smoother density contours obtained by the streamline PIC model are due to the fact that the random motion of beamlet ions are neglected with respect to the

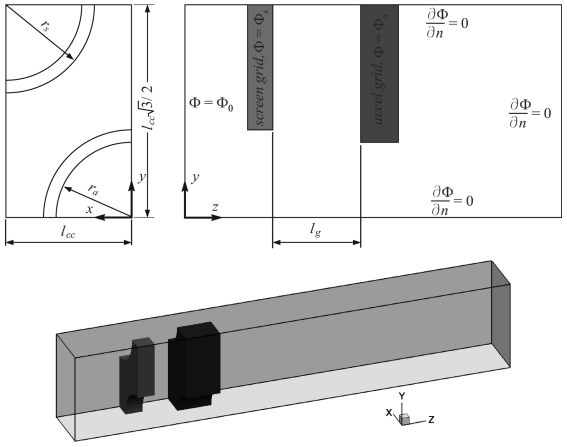

Fig. 7 Simulation setup of the ion optics plasma flow tests.

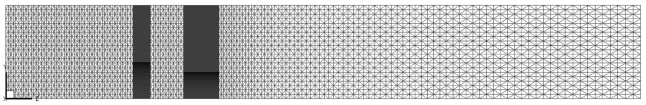

Fig. 8 IFE mesh used for the simulation of two quarter-apertures at $n_0 = 1.0 \times 10^{17}$ m^{-3}.

bulk motion. However, the beamlet focusing is almost the same as calculated by both models. The upstream sheath and beamlet focusing is the most important feature an ion optics model needs to resolve in order to determine the amount of extracted beamlet current and access grid impingement current. We find that neglecting the random motion of beamlet ions has a diminishing effect on ion beamlet simulation results because of the dominating effect of the external accelerating electrostatic field. Hence, it is acceptable to use the streamline HG-IFE-PIC model for ion optics simulations on beamlet behavior.

B. The Mesh Stretching Parameter

We next compare the solution of the HG-IFE-PIC obtained on a stretched IFE mesh with a base solution in which the IFE mesh is uniform. The stretching is done here only in the downstream zone along the z-direction. The solution of each stretched mesh is compared to the base solution. Figure 11 shows the L^2 norm of the difference between the solution of stretched mesh and that of the uniform mesh as a function of β

$$||\Delta\Phi||_2 = ||\Phi|_\beta - \Phi|_{\beta\to\infty}||_2 \tag{10}$$

From the plot, we notice that the error introduced by the mesh stretching becomes negligible for $\beta \geq 1.2$. Hence, $\beta = 1.2$ is used in the simulations shown in the next section.

IV. Modeling Whole Subscale Ion Optics Gridlet

A seven-aperture subscale ion optics gridlet model as shown in Fig. 12 is used as an example for the simulation study. The dimensions of this ion optics and the operating conditions considered are shown in Tables 1 and 2, respectively. These parameters are chosen to be similar to a prototype subscale ion optics designed and tested at Colorado State University. The accelerator grid and screen grid thickness of this gridlet model are 50% thicker than the NSTAR ion optics to allow for a longer service life.

The simulation model setup is similar to that discussed in [10]. The simulation domain is a three-dimensional rectangle domain that includes a quarter of the gridlet. This setup accounts for the geometric effects from a hexagonal layout of surrounded and circumferential apertures, and allows symmetric boundary conditions to be applied on planes of symmetry of the domain. In the beam flow direction, the upstream domain boundary is immersed in the discharge chamber plasma. We make no assumption about the upstream plasma sheath surface. The ion extraction is determined self-consistently from the acceleration voltage drop and the upstream plasma boundary conditions. The downstream domain boundary is placed in the neutralized propellant plasma. The last few cells next to the downstream boundary are considered as a quasi-neutral zone where the propellant ions are neutralized [10]. We take the downstream plasma density to be the average ion density within the quasi-neutral zone. Hence, the downstream plasma density is updated each time step.

Macroparticles representing the propellant beam ions are introduced into the simulation domain from the upstream boundary at each PIC time step. The trajectory of each ion is determined from the integration of its equation of motion given by Newton's second law as

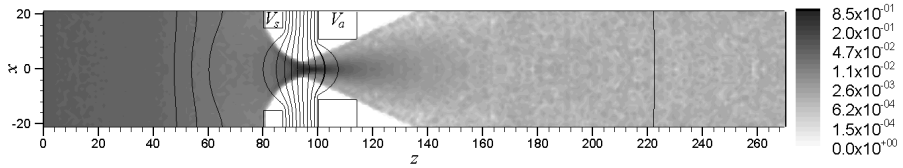

a) Cross-over, $n_0 = 0.05 \times 10^{17}$m^{-3}

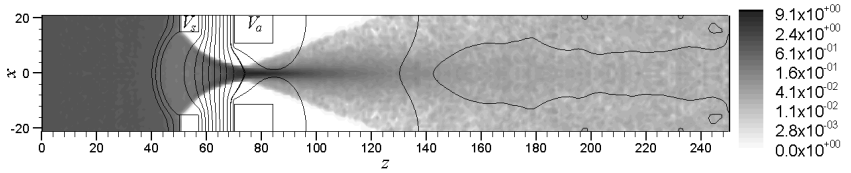

b) Normal, $n_0 = 1.0 \times 10^{17}$m^{-3}

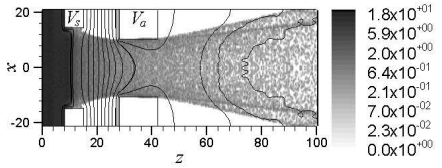

(c) Perveance, $n_0 = 14.0 \times 10^{17}$m^{-3}

Fig. 9 Standard PIC simulations: beamlet potential and ion density. Ion density is normalized by 1.0×10^{17} m^{-3}. Potential contour lines are shown for the values from −210 to 1790 V with a step of 200 V. The −140, 0, 1780, and 1795 V contour lines are also shown.

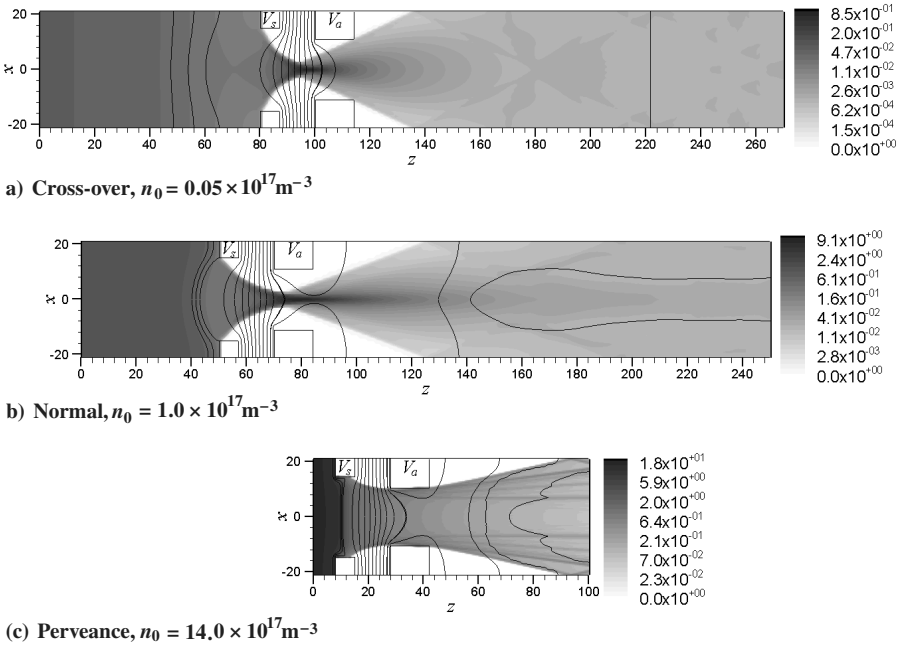

Fig. 10 Streamline PIC simulations: beamlet potential and ion density. Ion density is normalized by $n_0 = 1.0 \times 10^{17}$ m^{-3}. Potential contour lines are shown for the values from −210 to 1790 V with a step of 200 V. The −140, 0, 1780, and 1795 V contour lines are also shown.

$$\frac{\mathrm{d}}{\mathrm{d}t}(m\boldsymbol{v}) = \boldsymbol{F} = q\boldsymbol{E} \tag{11}$$

$$\boldsymbol{v} = \frac{\mathrm{d}\boldsymbol{x}}{\mathrm{d}t} \tag{12}$$

The electron density is considered to follow the Boltzmann distribution in the regions where electrons exist, i.e., the upstream and downstream regions of the ion optics. Specifically, in the upstream region, the electron density is given by

$$n_e = n_{e0} \exp\left(\frac{e(\Phi - \Phi_0)}{kT_{e0}}\right) \tag{13}$$

where Φ_0, n_{e0}, and T_{e0} are, respectively, the potential, electron density, and electron temperature of the discharge plasma. The downstream electron density is given by

$$n_e = n_{e\infty} \exp\left(\frac{e(\Phi - \Phi_\infty)}{kT_{e\infty}}\right) \tag{14}$$

where Φ_∞, $n_{e\infty}$, and $T_{e\infty}$ are, respectively, the potential, electron density and electron temperature of the downstream neutralized plasma. The electrostatic field is solved self-consistently with the boundary condition and the space charge of the particles from the Poisson's equation

$$\nabla \cdot (\epsilon_0 \nabla \Phi) = e(n_e - n_i) \tag{15}$$

As the focus of this study is to simulate the behavior of the acceleration grid impingement current and identify the crossover and the perveance limit, simulations presented here only concern the flow of the propellant beam ions. Charge-exchange ions generated between the beam ions and neutrals are not included in order to speed up the simulation. Charge-exchange ions have very little effect on the ion optics electric field and the beam ions trajectories because of their negligible contribution to the overall space charge. The inclusion of charge-exchange ions in the simulation will only change the magnitude of the impingement current slightly and is not expected to affect the crossover limit and the perveance limit.

We consider an upstream discharge plasma electron temperature $T_{e0} = 5$ eV, a downstream plasma potential $\Phi_\infty = 0$ and a downstream plasma electron temperature $T_{e\infty} = 1.5$ eV. The ion temperature in the discharge plasma is assumed to be equal to the discharge chamber temperature, $T_i = T_w \approx 300$ K. To calculate the beam ion extraction properly, the upstream boundary needs to be set far enough from the screen grid and the cell size should resolve the

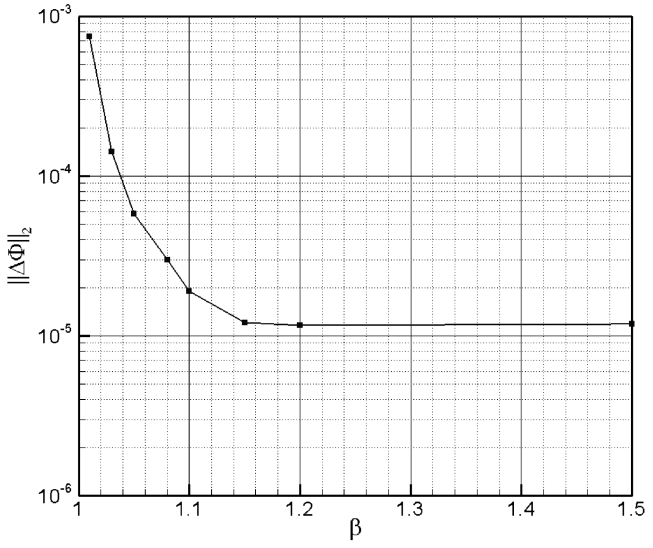

Fig. 11 Effect of stretching parameter on ion optics potential solution.

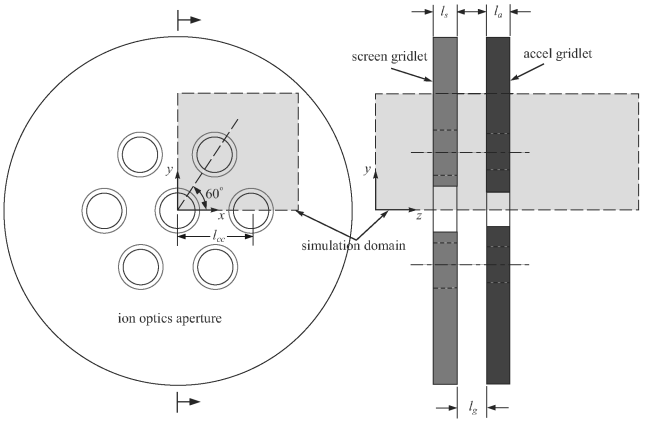

Fig. 12 Simulation domain of a whole subscale gridlet with seven apertures.

Table 1 Nominal dimensions of the ion optics

Screen hole diameter, d_s	0.0595 in	(1.511 mm)
Screen grid thickness, t_s	0.015 in	(0.381 mm)
Acceleration hole diameter, d_a	0.043 in	(1.092 mm)
Acceleration grid thickness, t_a	0.03 in	(0.762 mm)
Screen to acceleration grid gap, l_g	0.026 in	(0.66 mm)
Center-to-center hole spacing, l_{cc}	0.0874 in	(2.22 mm)

Table 2 Throttling condition of the ion optics

Net accelerating voltage, V_n	1800 V
Screen grid voltage, V_s	1780 V
Acceleration grid voltage, V_a	−210 V

Debye length of the upstream discharge plasma [10], λ_{D0}. For instance, for $T_{e0} = 5$ eV and nominal discharge plasma density of 1.0×10^{17} m^{-3}, the Debye length $\lambda_{D0} \approx 5.26 \times 10^{-5}$ m. Because $\lambda_{D0} \propto 1/\sqrt{n_0}$, a suitable PIC mesh needs to be used to simulate each discharge plasma density. In the simulations, the resolution of the uniform Cartesian PIC mesh varies for different upstream plasma conditions and is taken to be $h_z = \lambda_{D0}$. The upstream plasma density considered in this paper ranges from $n_0 = 0.05 \times 10^{17}$ to $n_0 = 14 \times 10^{17}$ m^{-3}. As the upstream plasma density increases, the upstream sheath boundary and the downstream beamlet mixing region will move closer towards the optics grid due to the smaller Debye length and thus the potential and plasma density gradient will be contained in a smaller region. Hence, we also vary the domain size in the z-direction for different upstream plasma conditions to save computation time. For instance, the upstream and downstream domain boundaries for the perveance condition run ($n_0 = 14 \times 10^{17}$ m^{-3}) are placed much closer to the optics grid than that for the crossover condition run ($n_0 = 0.05 \times 10^{17}$ m^{-3}). On the other hand, the perveance condition run requires a much higher mesh resolution and thus uses more total number of mesh points than the crossover condition run. Numerical tests were performed to ensure that the locations of the upstream and downstream domain boundary have no effects on the simulation results.

As the beam ion density decreases rapidly in the downstream region of the acceleration grid, we allow the IFE mesh to stretch gradually in the downstream region. The stretched IFE mesh is such that $\Delta z_{\min} = \lambda_{D0}$ and $\Delta z_{\max} < \lambda_{D\infty}$, where Δz is the length of the IFE base Cartesian cells in the z-direction. As discussed in the preceding section, the stretching parameter used in all cases is 1.2 (see Fig. 11). In the lateral directions, we use a uniform mesh size. The IFE mesh used for the simulation run of $n_0 = 1.0 \times 10^{17}$ m^{-3} is shown in Fig. 13. Table 3 summarizes the mesh parameters for all runs.

All simulation runs in this paper were performed on a Dell® Workstation with dual Intel® Xeon™ processors at 3.0 GHz and 2 GB total memory. The computational time required to reach steady-state ion trajectories depends on the upstream plasma condition. It varies from less than 3 h, for densities much less than the crossover limit, to over 60 h for densities much larger than the perveance limit. The number of particles injected each simulation loop was 156,600 particles in all runs. It is worth noting here that the application of the HG-IFE-PIC algorithm significantly speeds up three-dimensional PIC ion optics simulations. Simulations of the entire operation envelope can be completed in a matter of days using regular PCs.

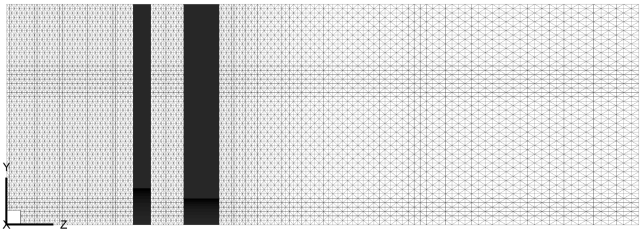

Fig. 13 IFE mesh used for the simulation of whole gridlet at $n_0 = 1.0 \times 10^{17}$ m^{-3}.

V. Simulation Results

A. Beamlet Behavior

To investigate the operation envelope of the ion optics grid, the beamlet current was varied over a wide range from below the crossover limit to above the perveance limit. The beamlet current, which is an important parameter in ion optics studies, was varied by changing the upstream plasma density from 0.05×10^{17} up to 14.0×10^{17} m^{-3}.

The potential and beamlet ion density contours on the $y = 0$ plane, which represents the horizontal plane cutting through the middle of the gridlet, are shown in Figs. 14–16 for the nominal, crossover, and perveance conditions, respectively. Comparing these results with the potential and density contours obtained using a single-aperture model (the two quarter-apertures setup) shown in Fig. 10, the differences between an edge aperture and a central aperture are obvious.

From Figs. 14–16, we can also distinguish the upstream plasma sheath (shown by the potential contour of $\Phi = \Phi_s$, where Φ_s is the screen grid potential). We notice that the shape and size of the sheath changes drastically with the variation in the upstream density. An accurate estimation of the size and shape of the upstream plasma sheath is of crucial importance to ion optics studies because it determines the ion extraction of an ion optics grid set. For example, at the nominal upstream density, the upstream plasma sheath is attached to the screen grid, and moderately dished with a convex and nearly spherical upstream side. If the upstream density is reduced to much lower than the nominal density, the upstream sheath becomes detached from the screen grid. If the upstream density is increased to much higher than the nominal density, the upstream sheath will be pushed by the dense upstream plasma towards the screen aperture to the extent that it sits at the aperture opening.

For the normal condition and the perveance limit cases, we find that the beamlet through the edge aperture has a similar profile to that of the center aperture. These profiles are also similar to the results from the single-aperture model. However, for the crossover case, the beamlet through the edge aperture is asymmetrically focused more towards the optics center. As a result, the edge aperture of the accel grid experiences significant direct beam ion impingement on the portion oriented towards the center, whereas the other parts of the accel grid see almost no direct impingement (Fig. 15). The distortion on the edge aperture beamlet is more significant for the crossover case because there is less Debye shielding at lower plasma densities and hence, the asymmetric electric field from optics grid can penetrate deeper into the beamlet. Figure 17 plots the distribution of

Table 3 PIC and IFE meshes used in the streamline HG-IFE-PIC whole gridlet simulation as a function of the upstream plasma density

Plasma density $\times 10^{17}$, m^{-3}	PIC mesh		IFE mesh	
	h_z, m	$n_x \times n_y \times n_z$	$n_x \times n_y \times n_z$	Elements
$0.05 \le n_0 \le 1.0$	5.2566×10^{-5}	$88 \times 51 \times 271$	$88 \times 51 \times 191$	4,132,500
$2.0 \le n_0 \le 4.0$	2.6283×10^{-5}	$175 \times 101 \times 341$	$175 \times 101 \times 127$	10,962,000
$6.0 \le n_0 \le 10.0$	1.7522×10^{-5}	$175 \times 101 \times 331$	$175 \times 101 \times 100$	8,613,000
$12.0 \le n_0 \le 14.0$	1.3142×10^{-5}	$175 \times 101 \times 401$	$175 \times 101 \times 116$	10,005,000

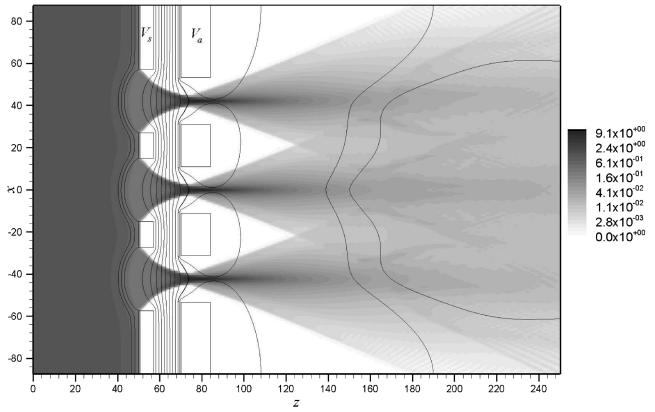

Fig. 14 Streamline PIC whole ion optics simulations (normal, $n_0 = 1.0 \times 10^{17}$ m^{-3}): beamlet potential and ion density. Ion density is normalized by 1.0×10^{17} m^{-3}. Potential contour lines are shown for the values from −210 to 1790 V with a step of 200 V. The −140, 0, 1780, and 1795 V contour lines are also shown.

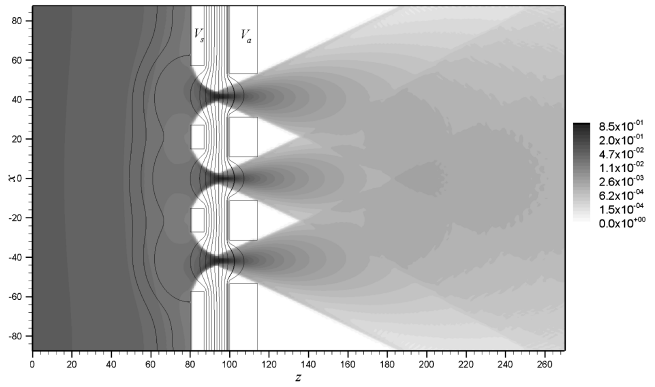

Fig. 15 Streamline PIC whole ion optics simulations (crossover, $n_0 = 0.05 \times 10^{17}$ m^{-3}): beamlet potential and ion density. Ion density is normalized by 1.0×10^{17} m^{-3}. Potential contour lines are shown for the values from −210 to 1790 V with a step of 200 V. The −140, 0, 1780, and 1795 V contour lines are also shown.

beam ion impingement on the inside wall of the edge aperture of the accel grid, showing that direct impingement is asymmetrically concentrated on the inboard portion of the aperture. This result indicates that, when an ion optics operates near the crossover limit, significant sputtering erosion would first occur to the edge apertures of the accel grid, and the erosion pattern on the edge apertures would be very asymmetrical.

B. Impingement Current Limits

By varying the upstream plasma density, we can scan the operating envelope of an ion optics grid set and determine the crossover and perveance limits. For each upstream density, the accel grid impingement current, I_i, is calculated as well as the beamlet current, I_b, itself. The ratio of the impingement current of the accel grid to the beamlet current, I_i/I_b, is plotted against the upstream density and beamlet current in Fig. 18. From the plots, we notice that the impingement current is zero over a wide range of upstream plasma densities, or beamlet currents. This range defines the *feasible* operating range of the ion optics grid set. From Fig. 18, we notice that the single-aperture model predicts the crossover limit at $I_b \simeq 0.017$ mA and the perveance limit at $I_b \simeq 0.469$ mA. The seven-apertures model predicts the crossover limit at $I_b \simeq 0.02$ mA and the perveance limit at $I_b \simeq 0.464$ mA. As the density, or beamlet current, goes beyond these limits, the impingement current increases. The crossover predicted by the multiple aperture model is about 17.6% over the prediction from the single-aperture model. This difference is due to direct impingement on the edge aperture

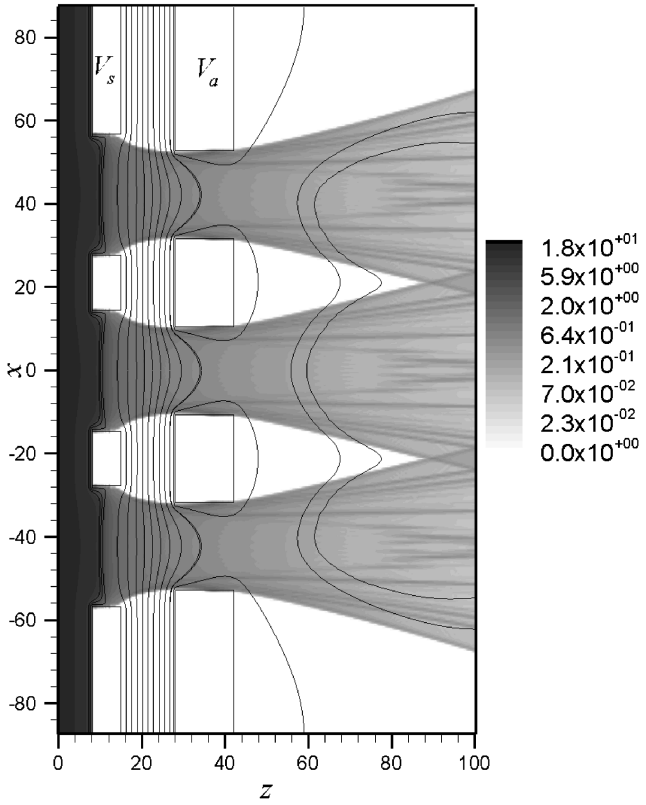

Fig. 16 Streamline PIC whole ion optics simulations (perveance, $n_0 = 14.0 \times 10^{17}$ m^{-3}): beamlet potential and ion density. Ion density is normalized by 1.0×10^{17} m^{-3}. Potential contour lines are shown for the values from −210 to 1790 V with a step of 200 V. The −140, 0, 1780, and 1795 V contour lines are also shown.

discussed in the preceding section. Ongoing experimental work performed at Colorado State University (CSU) on several gridlet sets provides measurements for the crossover and perveance limits operated at several throttling values [18,19]. The comparison of our modeling results against CSU experimental results will be presented in a future study.

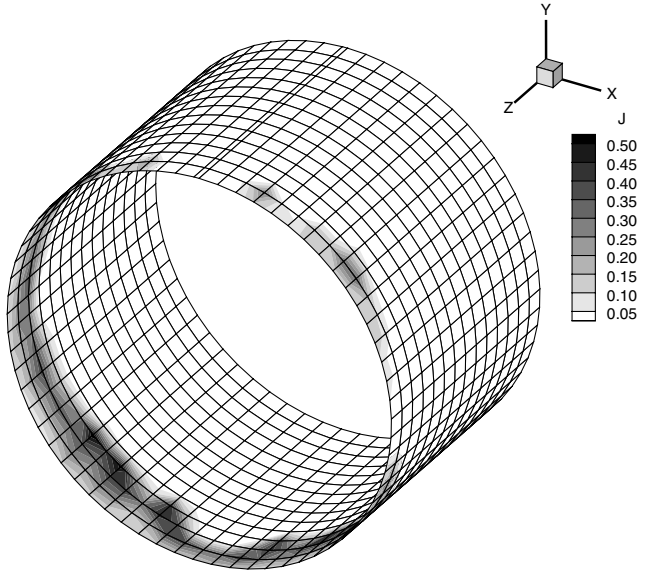

Fig. 17 Beam ion impingement current density distribution on the edge aperture wall of accel grid at crossover ($n_0 = 0.05 \times 10^{17}$ m^{-3}). The view angle is from the downstream side of the accel grid. (Contour level unit: mA/mm^2).

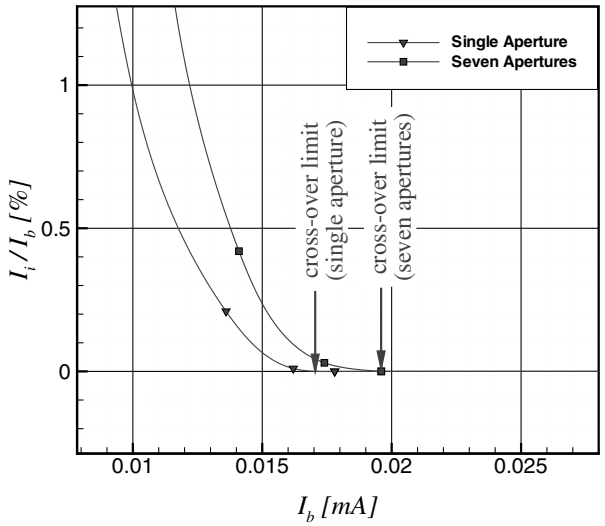

a) Cross-over limit

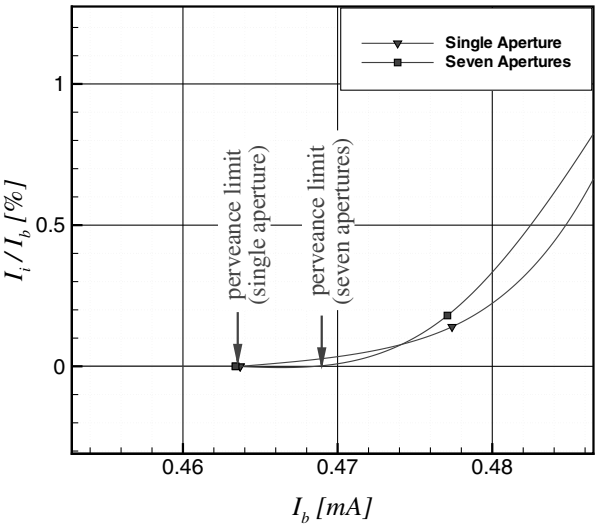

b) Perveance limit

Fig. 18 Impingement current limits.

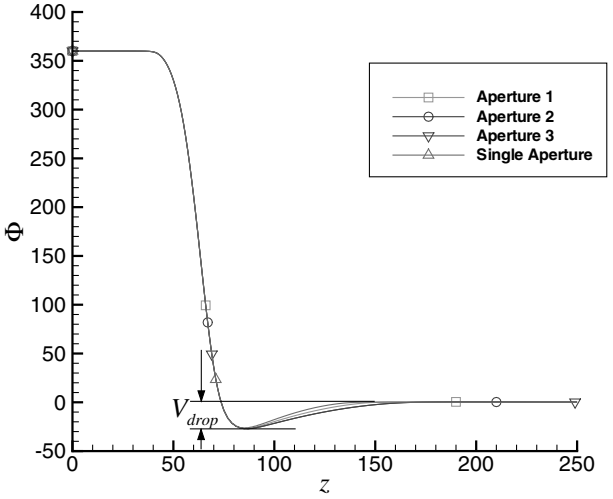

Fig. 19 Potential profile along aperture centerlines.

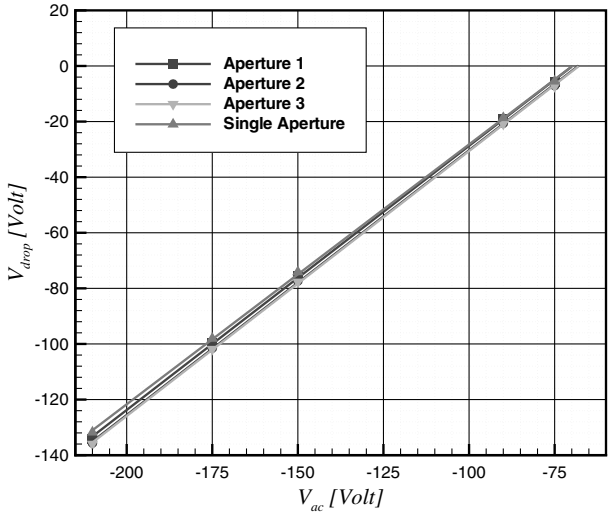

Fig. 20 Electron backstreaming limit.

C. Electron Backstreaming

This new model can also be applied to estimate the onset of electron backstreaming. Here, the onset of electron backstreaming in a certain gridlet aperture is defined as the condition when the potential profile along the aperture centerline becomes monotonic. At such a condition, the potential well downstream of the accel grid which prevents the neutralization electrons far downstream from backflowing towards the accel grid disappears. In this paper, we do not study electron backstreaming due to the enlargement of the accel grid aperture. We only consider electron backstreaming due to changes of the accel grid voltage. Simulations are performed for various accel grid voltages using both the whole ion optics gridlet model and the single-aperture model. The potential profiles along the centerline of each aperture of the whole gridlet model are compared with that of the single-aperture model in Fig. 19. The voltage drops along the centerline of the apertures are plotted against the accel grid voltage in Fig. 20. We find that the electron backstreaming limit for the central aperture in the seven aperture model is very close to that predicted by the single-aperture model. However, the backstreaming limit for the circumferential apertures is different from the center aperture by about 2 V. The difference in electron backstreaming between the single-aperture and the whole ion optics models is not as predominant as in ion beamlet behavior. This is because the electrons are influenced more by the random thermal motion whereas the ions primarily follow the directed flow under the electric field. Hence, the effects from the asymmetry in electric field near the grid are more obviously reflected in ion dynamics.

VI. Summary and Conclusions

A new ion optics model is introduced for three-dimensional global simulations of plasma flow in an entire subscale ion optics gridlet. This model explicitly includes apertures located near the edge of the grid surface and fully accounts for the effects of multiple ion beamlets and geometric asymmetry. This model is based on a new algorithm, the streamline hybrid-grid immersed-finite-element particle-in-cell (HG-IFE-PIC). The HG-IFE-PIC algorithm is capable of achieving the same accuracy of an unstructured body-fit mesh-based particle-in-cell but at a faster computational speed. As a result, the calculation of the performance envelope from the crossover to the perveance limits for a multiple aperture subscale ion optics gridlet can be accomplished in a few days using regular PCs. Simulations are carried out for a model seven-aperture optics gridlet and results are compared with that from a single-aperture model. Whereas a single-aperture model is adequate for modeling an aperture located in the center of the optics grid, it cannot resolve the quantitative differences in plasma sheath and beamlet behavior between the center aperture and the circumferential apertures. We find that the whole ion optics model would predict a higher beamlet current for both the crossover and the perveance limit as well as a slightly higher accelerator grid voltage for electron backstreaming

onset than the single-aperture model. The differences between the single-aperture model and the whole ion optics model is most predominant in ion beamlet at crossover. The ion beamlets through circumferential apertures are focused more towards the optics center due to the asymmetry in electric field near the grid surface. Hence, when an ion optics operates near the crossover condition, its accel grid would experience significant direct ion impingement concentrated on the aperture side oriented towards the optics center.

Acknowledgments

We acknowledge useful discussions with John Williams of Colorado State University on ion optics experiments and the contributions of Yong Cao and Tao Lin of Virginia Tech to the development of the simulation model.

References

[1] Birdsall, C. K., and Langdon, A. B., *Plasma Physics Via Computer Simulation*, Series in Plasma Physics, Inst. of Physics Publishing, London, 1991.

[2] Peng, X., Keefer, D., and Ruyten, W., "Plasma Particle Simulation of Electrostatic Ion Thrusters," *Journal of Propulsion and Power*, Vol. 8, No. 2, 1992, pp. 361–366.

[3] Hayakawa, Y., "Three-Dimensional Numerical Model of Ion Optics System," *Journal of Propulsion and Power*, Vol. 8, No. 1, 1992, pp. 110–117.

[4] Arakawa, Y., and Nakano, M., "An Efficient Three-Dimensional Optics Code for Ion Thruster Research," AIAA Paper 96-3198, July 1996.

[5] Tartz, M., Hartmann, E., Deltaschew, R., and Neumann, H., "Grid Erosion Study of a Three-Dimensinal Ion Thruster," AIAA Paper 98-3646, July 1998.

[6] Muravlev, V. A., and Shagayda, A. A., "Numerical Modelling of Extraction Systems in Ion Thrusters," IEPC Paper 99-162, July 1999.

[7] Okawa, Y., and Takegahara, H., "Particle Simulation on Ion Beam Extraction Phenomena in an Ion Thruster," IEPC Paper 99-146, July 1999.

[8] Boyd, I. D., and Crofton, M. W., "A Computational Study of Grid Erosion Through Ion Impact," AIAA Paper 00-3664, July 2000.

[9] Nakayama, Y., and Wilbur, P. J., "Numerical Simulation of Ion Beam Optics for Multiple-Grid Systems," *Journal of Propulsion and Power*, Vol. 19, No. 4, 2003, pp. 607–613.

[10] Wang, J., Polk, J., Brophy, J., and Katz, I., "Three-Dimensional Particle Simulations of Ion-Optics Plasma Flow and Grid Erosion," *Journal of Propulsion and Power*, Vol. 19, No. 6, 2003, pp. 1192–1199.

[11] Farnell, C. C., Williams, J. D., and Wilbur, P. J., "NEXT Ion Optics Simulation via ffx," AIAA Paper 03-4869, July 2003.

[12] Farnell, C. C., Williams, J. D., and Wilbur, P. J., "Numerical Simulation of Ion Thruster Optics," NASA CR-212305, July 2003.

[13] Farnell, C., "Numerical Simulation of HiPEP Ion Optics," AIAA Paper 04-3818, July 2004.

[14] Anderson, J., Katz, I., and Goebel, D., "Numerical Simulation of Two-Grid Ion Optics Using a 3D Code," AIAA Paper 04-3814, July 2004.

[15] Emhoff, J. W., and Boyd, I. D., "Grid Erosion Modeling of the NEXT Ion Thruster Optics," AIAA Paper 03-4868, July 2003.

[16] Emhoff, J. W., and Boyd, I. D., "Progress in NEXT Ion Optics Modeling," AIAA Paper 04-3786, July 2004.

[17] Emhoff, J. W., and Boyd, I. D., "NEXT Ion Optics Modeling of Total Thruster Performance," AIAA Paper 05-3687, July 2005.

[18] Laufer, D. M., Williams, J. D., Farnell, C. C., Shoemaker, P. B., and Wilbur, P. J., "Experimental Evaluation of Sub-Scale CBIO Ion Optics Systems," AIAA Paper 03-5165, July 2003.

[19] Martinez, R. A., Buttweiler, M. S., and Williams, J. D., "Evaluation of Sub-Scale NEXIS Ion Optics and Strategies for Performing Accelerated Wear Testing," AIAA Paper 04-3628, July 2004.

[20] Kafafy, R., Lin, T., Lin, Y., and Wang, J., "Three Dimensional Immersed Finite Element Methods for Electric Field Simulation in Composite Materials," *International Journal for Numerical Methods in Engineering*, Vol. 64, Aug. 2005, pp. 940–972.

[21] Kafafy, R., Lin, T., and Wang, J., "3-Dimensional Ion Optics Simulations Using an IFE-PIC Code," AIAA Paper 03-5164, July 2003.

[22] Wang, J., Cao, Y., Kafafy, R., Pierru, J., and Decyk, V., "Ion Propulsion Simulations Using Parallel Supercomputer," IEPC Paper 05-271, Oct. 2005.

[23] Kafafy, R., and Wang, J., "A Hybrid-Grid Immersed-Finite-Element Particle-in-Cell Algorithm for Modeling Spacecraft Plasma Interactions," *IEEE Transactions on Plasma Science*, (accepted for publication).

[24] Wang, J., Polk, J., Brophy, J., and Katz, I., "3-D Particle Simulations of NSTAR Ion Optics," IEPC Paper 01-085, Oct. 2001.

[25] Ewing, R. E., Li, Z., Lin, T., and Lin, Y., "The Immersed Finite Volume Element Methods for the Elliptical Interface Problems," *Mathematics and Computers in Simulation*, Vol. 50, Nos. 1–4, Nov. 1999, pp. 63–76.

[26] Lin, T., Lin, Y., Rogers, R., and Ryan, M. L., "A Rectangular Immersed Finite Element Space for Interface Problems," *Advances in Computation: Theory and Practice*, Nova Science Publishers, Commack, NY, 2001, pp. 107–114.

[27] Mandell, M. J., and Katz, I., "High-Voltage Plasma Interactions Calculations Using NASCAP/LEO," AIAA Paper 90-725, Jan. 1990.

[28] Mandell, M. J., Katz, I., Hilton, J. M., Minor, J., and Cooke, D. L., "NASCAP2K—A Spacecraft Charging Analysis Code for the 21st Century," AIAA Paper 01-957, Jan. 2001.

[29] Kafafy, R., "Immersed Finite Element Particle-In-Cell Simulations of Ion Propulsion," Ph.D. Dissertation, Virginia Polytechnic Institute and State University, Blacksburg, VA, Sept. 2005.

[30] Chung, T. J., *Computational Fluid Dynamics*, Cambridge Univ. Press, Cambridge, England, 2001.

[31] Nakayama, Y., and Wilbur, P. J., "Numerical Simulation of Ion Beam Optics for Many-Grid Systems," AIAA Paper 01-3782, July 2001.

[32] Brophy, J. R., Katz, I., Polk, J. E., and Anderson, J. R., "Numerical Simulations of Ion Thruster Accelerator Grid Erosion," AIAA Paper 02-4261, July 2002.

R. Myers
Associate Editor